



## OPEN ACCESS

## EDITED BY

Saji Uthaman,  
Iowa State University, United States

## REVIEWED BY

Yong-Qu Zhang,  
Xiamen University, China  
Ming-Hsien Chan,  
Academia Sinica, Taiwan

## \*CORRESPONDENCE

Xiaobo Wang  
VitaDrwang@cdutcm.edu.cn  
Xianli Meng  
xlm999@cdutcm.edu.cn

## SPECIALTY SECTION

This article was submitted to  
Cancer Imaging and  
Image-directed Interventions,  
a section of the journal  
Frontiers in Oncology

RECEIVED 06 July 2022

ACCEPTED 18 August 2022

PUBLISHED 08 September 2022

## CITATION

Fan F, Hou Y, Zhang Y, Zeng Y,  
Zhang Y, Zhang S, Meng X and Wang X  
(2022) Tumor imaging and  
photothermal therapy in second near  
infrared window: A systematic review  
and meta-analysis.  
*Front. Oncol.* 12:987491.  
doi: 10.3389/fonc.2022.987491

## COPYRIGHT

© 2022 Fan, Hou, Zhang, Zeng, Zhang,  
Zhang, Meng and Wang. This is an  
open-access article distributed under  
the terms of the [Creative Commons  
Attribution License \(CC BY\)](https://creativecommons.org/licenses/by/4.0/). The use,  
distribution or reproduction in other  
forums is permitted, provided the  
original author(s) and the copyright  
owner(s) are credited and that the  
original publication in this journal is  
cited, in accordance with accepted  
academic practice. No use,  
distribution or reproduction is  
permitted which does not comply with  
these terms.

# Tumor imaging and photothermal therapy in second near infrared window: A systematic review and meta-analysis

Fuhan Fan<sup>1</sup>, Ya Hou<sup>1</sup>, Yating Zhang<sup>1</sup>, Yong Zeng<sup>1</sup>, Yi Zhang<sup>2</sup>, Sanyin Zhang<sup>3</sup>, Xianli Meng<sup>1,2,3\*</sup> and Xiaobo Wang<sup>1\*</sup>

<sup>1</sup>School of Pharmacy, Research Institute of Integrated TCM & Western Medicine Chengdu University of Traditional Chinese Medicine, Chengdu, China, <sup>2</sup>Ethnic Medicine Academic Heritage Innovation Research Center, Chengdu University of Traditional Chinese Medicine, Chengdu, China, <sup>3</sup>State Key Laboratory of Southwestern Chinese Medicine Resources, Innovative Institute of Chinese Medicine and Pharmacy, Chengdu University of Traditional Chinese Medicine, Chengdu, China

**Background:** Second near-infrared window (NIR-II, 1000-1700 nm) technology for tumor imaging and photothermal therapy (PTT) is an innovative method for tumor diagnosis and treatment. The NIR-II probe can specifically identify tumor cells, and effectively convert light energy into heat energy under the irradiation of NIR laser, thus achieving the integration of non-invasive tumor diagnosis and treatment. In the present study, we conducted a systematic review and meta-analysis of preclinical investigations to corroborate the efficacy and safety of photothermal therapy.

**Methods:** Relevant preclinical data were retrieved by searching PubMed, Web of Science, CNKI, WANFANG and VIP information databases. And the acquired data were analyzed by RevMan Version 5.3 software.

**Results:** According to the inclusion criteria, forty-two articles relating to NIR-II tumor imaging and PTT were recruited for further in-depth analysis. The NIR-II photoacoustic and fluorescence imaging could quickly and accurately identify tumor in mice, manifesting higher signal intensity on tumor site than that of normal tissue. After PTT, the tumor volume of mice decreased miraculously [RR=8.49, 95%CI (4.64, 15.55), P<0.00001], and even disappeared completely [RR=7.01, 95%CI (3.04, 16.13), P<0.00001] with no potential risk of affecting the blood routine.

**Conclusions:** PTT guided by NIR-II imaging can effectively diagnose the tumor lesion and eliminate it with the advantages of non-invasive and higher biosafety.

## KEYWORDS

NIR-II, tumor imaging, photothermal therapy, safety evaluation, meta-analysis

## Introduction

Tumor is a form of disease with excessive mortality globally with no effective and completely acceptable techniques for its cure and prognosis (1). Conventional non-invasive medical imaging devices, such as computed tomography (CT), magnetic resonance imaging (MRI), ultrasound (US) and positron emission tomography (PET) (2), have made some achievements in the detection of diversified tumors. However, the problems of low resolution, shallow imaging depth and inevitable radiation still force human beings to hunt for novel clinical imaging methods, which stimulate a new development in optical imaging. It is well worth noting that photons for biological imaging in visible light window will be scattered and absorbed by blood, fat and hemoglobin in organic tissues, making it difficult to photograph deep tissues (3). As a result, near-infrared (NIR) imaging and therapeutic methods with robust tissue penetration and small photons scattering have been swiftly developed in current years. Imaging guided *via* the first near infrared window (NIR-I, 700-900nm) and the NIR-II window is the predominant direction of NIR imaging (4). Even more thrillingly, the greater imaging depth and signal-to-noise ratio of the NIR-II window make it extra competitive in contrast with the NIR-I window (5). As a promising technology for tumor diagnosis, NIR-II fluorescence can label specific tissue structures at the molecular or cellular level, contributing to identify minimal residual tumors with high precision.

In addition, some NIR probes can additionally be used as photothermal agents (PTA) to achieve photothermal therapy (PTT) of tumor cells under the irradiation of NIR laser (6). PTT is a cure approach that kills tumor cells by way of heating up the local tumor tissue. It has been reported that irreversible injury can be brought about to tumor cells when the temperature exceeds 43°C (7). The tumor site was accurately located by NIR-II imaging system *via* certain NIR laser irradiation to the tumor tissue. In principle, PTA can activate from ground state to excited state by absorbing photon energy under NIR laser irradiation, and then collide with surrounding molecules to generate kinetic energy and eventually convert into heat to kill tumor cells (8). After a persistent period of photothermal treatment, blood and major organs of tumor model mice were collected for blood routine and H&E staining analysis. It was suggested that a mass of the tumor cells went into apoptosis with no distinct difference in normal tissue and blood routine indexes between PTT-treated mice and normal mice (9, 10). Compared with traditional surgical resection for tumor treatment, NIR-II guided tumor imaging and PTT exhibit much less biological trauma and higher specificity (11), which was promising to be a novel approach for clinical treatment of tumors. The principles of tumor localization and photothermal treatment guided by NIR-II imaging are shown in Figure 1.

At present, NIR-II fluorescence imaging has made a great breakthrough in guiding clinical tumor resection. With the advantages of real-time imaging and wide field of view, it can provide dynamic feedback of tumor area information in the course of surgery. More accurately, numerous evidence demonstrated that NIR-II imaging can detect tumor signals that cannot be identified by CT imaging (12). Based on the achievements of NIR-II imaging in cancer surgery and the encouragement of preclinical data on photothermal treatment, we believe that NIR-II imaging guided PPT has a bright future in clinical cancer diagnosis and treatment. Due to the lack of relevant clinical data, we conducted a systematic review and meta-analysis of the preclinical data of PTT, providing more powerful evidence for its efficacy and safety.

## Methods

### Literature search

Two researchers (FF and YH) used PubMed, Web of Science, China National Knowledge Infrastructure (CNKI), WANFANG, and VIP Journal database to conduct a comprehensive search for publications up to January 10, 2022. The following is the literature search algorithm: (second near infrared OR NIR-II) AND (cancer OR tumor) AND (photothermal therapy OR PTT). In addition, there are no other relevant restrictions in the retrieval of literature search.

### Study selection

All the literatures were retrieved by the above programmed algorithm and were input into reference management software for unified management. Firstly, articles were preliminarily screened according to the title and abstract, and then the full context was read to cautiously consider whether to be subordinated to our study. Article selection criteria were carefully determined and strictly enforced during the study selection process. Studies were included when they conformed all of the following criteria: 1) Use of NIR-II imaging to locate tumors and cancer cells; 2) PTA related characterization; 3) Photothermal tests were carried out on mice using NIR-II imaging system, and data related to the efficacy and safety of PTT were obtained. Meanwhile, studies were excluded if they accorded with any of the following criteria: 1) One of a range of reviews, case reports, conference articles, abstracts, social reviews, and clinical literature; 2) None of experimental study; 3) None of NIR-II imaging; 4) None of records associated to the characteristic of PTA; 5) None of information related to tumor imaging; 6) None of data related to PTT; 7) Duplicate publications.

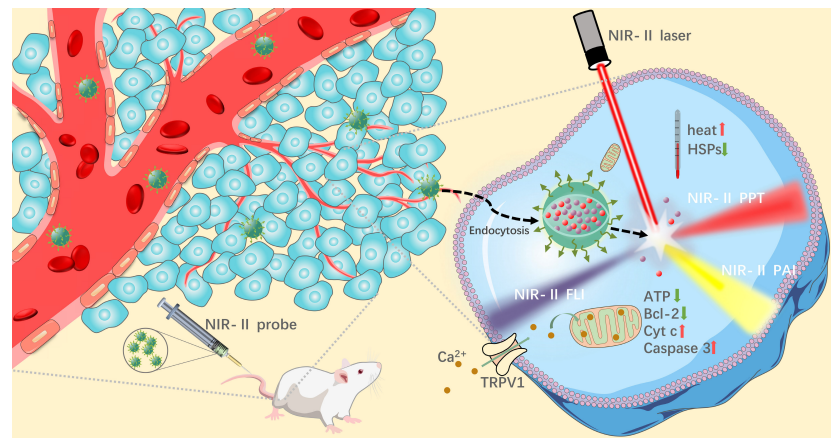


FIGURE 1  
Schematic diagram of tumor imaging and PTT in the second near-infrared window.

## Data extraction and quality evaluation

The process of information extraction was mutually performed by two reviewers (FF and YZ). Pre-defined information extraction strategies were employed for effective extraction, and the differences between reviewers were resolved by consensus. The required data was extracted as comprehensively as possible from the included article, including text material and charts as sources of information. However, when solely charts were available in the article, the applicable information was thus obtained quantitatively on the charts using the line length tool in PowerPoint (13). The essential information collected were as follows: first author and publication time, basic information of the PTA, bioactivity of the probe, tumor imaging ability, *in vitro* tissue signals, *in vitro* and *in vivo* photothermal conversion parameters of the PTA, grouping and sample size, photothermal treatment conditions, and volume change of tumor after PTT.

The quality of the studies was evaluated through scoring 10 indicators in the preclinical research quality evaluation table: 1) Whether the articles were published after peer review; 2) Whether there is a description of temperature control; 3) Whether animal groups are randomly assigned; 4) Whether to follow the allocation hiding; 5) Whether the outcome indicators were evaluated by blind method; 6) Whether anesthetics with neuroprotective properties are used; 7) Whether animal models with comorbidities are used; 8) Whether to specify the sample size; 9) Whether there is a declaration of animal welfare regulations (10); Whether there is a conflict of interest related declaration. When there is a description in the article that conforms to the relevant indicators, it will get one point under this indicator. Otherwise, it will no longer get point. The

ultimate rating of the paper was 0-10, with higher scores indicating more rigorous methodological design of research.

## Statistical analysis

RevMan version 5.3 software was used for data summary and analysis. Dichotomous variable method was used to characterize the efficacy of PTT in tumor treatment. The random-effects model and 95% confidence interval (CI) risk ratio (RR) were used to show the association. The continuous variable method was used to characterize the safety of PTT. Fixed effect model and mean difference (MD) of 95% CI were used to evaluate the changes of specific blood routine indexes. The  $I^2$  statistical test was used to test the heterogeneity of individual studies. When  $I^2 > 50\%$  of the time, we thought the study had significant heterogeneity. While the probability value less than 0.05 was considered statistically significant.

## Results

### Literature search

A total of 6299 related studies were obtained from the target database by the predefined search algorithm. And 5924 articles were retrieved by excluding duplicate articles. By reading the title and abstract of the articles, 5860 articles that did not conform the requirements were initially excluded, including 309 non-experimental articles, 120 informal articles (news reports and comments), 2860 articles that did not involve NIR-II imaging, 2338 articles that did not contain tumor imaging, and 134

articles that did not use PPT. The remaining 64 studies were then screened and evaluated through full-text reading, and 22 papers were further excluded. Finally, 42 related studies were included in the meta-analysis (7–10, 14–51). The retrieval and selection process of the article is shown in Figure 2.

## Study characteristics

Different kinds of probes have widespread differences in the outcomes of PTT. We sorted out the essential traits of the probes concerned in the studies (Table 1), including excitation wavelength, quantum yield (QY) and extinction coefficient ( $\epsilon$ ), et al. Due to the innovativeness of NIR-II image-guided PTT utilized to tumors treatment, all the included studies were published in latest years (2018 to 2021) and were preclinical researches. The type of probe imaging comprised NIR-II fluorescence imaging (21 researches), NIR-II photoacoustic imaging (6 researches), and NIR-II fluorescence photoacoustic dual-mode imaging (15 researches). The probes involved in each study were reported for the first time and were no longer reproducible with each other.

The emission wavelength, QY and  $\epsilon$  of the probe are considered as vital elements affecting the fluorescence brightness of the probe. QY refers to the fluorescence conversion rate of fluorescent probe after absorption of photons (52). Included in the literature studied in this paper, the highest QY of the probe is 3.78% (51), while the lowest is 0.004% merely (30). Almost all of the probes involved in the studies had the maximum emission peak in the NIR-II region, despite of a few of the probes (37, 40, 43) with no maximum emission peak in the NIR-II region, but still had a large amount of fluorescence emission in this region. The  $\epsilon$  of the probe at the maximum emission wavelength was further measured, and the

maximum and minimum  $\epsilon$  of the articles included in this paper were 130.3 and 2.01 L/cm $\cdot$ g (14, 24), respectively. In addition, the cell viability of probes with different concentrations and related cells cultured for a certain period of time was calculated as the important biosafety evaluation index of probes. The cell survival rate of the probes used in this study was above 80%, and the influence of some probes on cell activity even could be ignored (16, 24, 26, 46, 49).

## Tumor imaging capability of NIR-II

The probe is the basis of PTT for high-precision imaging of tumors in the NIR-II imaging system. In this regard, we thus sorted out the imaging information of different probes in Table 2. The capacity of the probe to image tumor can be expressed by the time of the maximum signal of NIR-II fluorescence imaging or photoacoustic imaging, and the ratio of the maximum signal to the initial signal. The shorter time of the maximum signal intensity indicated the stronger selectivity of the probe to the tumor. And the larger ratio of the maximum signal to the initial signal manifested the potential of imaging to a certain extent. In this paper, the maximum signal time of the fluorescent probe is mostly 12 h and 24 h, the shortest and longest time are 3 h (49) and 5 d (44) respectively. Noteworthy, the ratio of the maximum signal to the initial signal can be enhanced up to 15 times (40). Most of the time of the maximum signal of the photoacoustic probe is between 6–24 h with the ratio of the maximum signal to the initial signal up to about 13 times (17, 47).

In general, intravenously injected probes can image biological blood vessels to varying degrees. The smaller the visualized vessels by NIR-II imaging system indicates the higher accuracy of the probe to some extent. Most of the probes

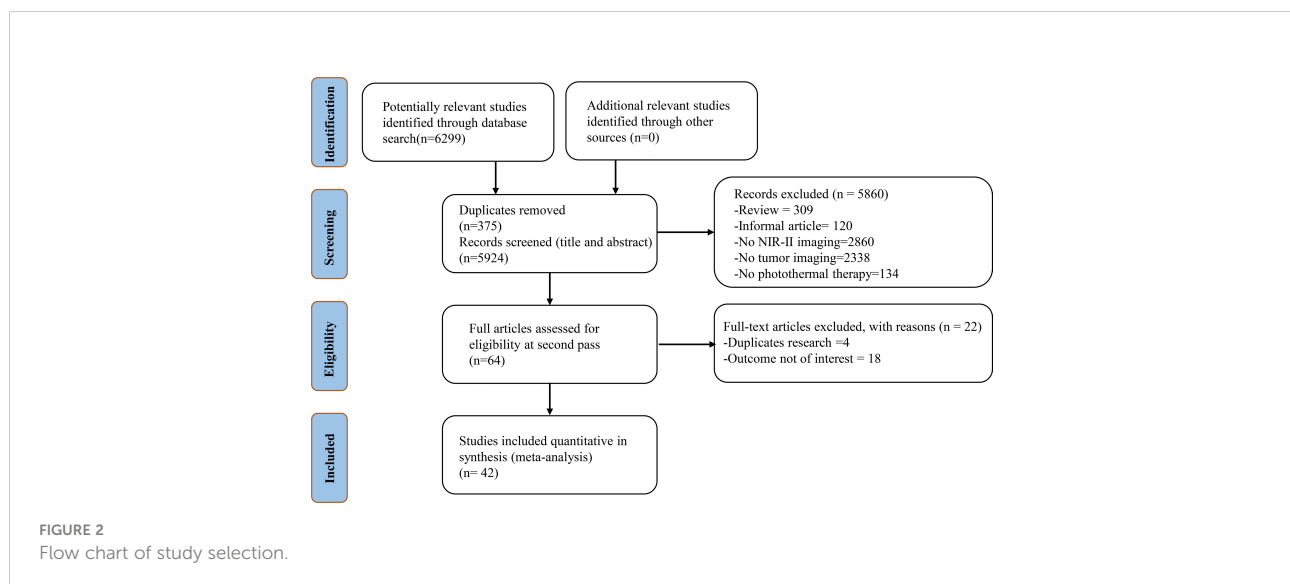


TABLE 1 The basic information of NIR-II probe included in the study.

Study	Names	Shape	Size (nm)	Type	A <sub>max</sub> (nm)	E <sub>max</sub> (nm)	QY (%)	ε (L/g.cm)	Cells Administration	Viability
Zhang 2021 (7)	SH-PEG-FA	Flake	37.6×1.5	PAI	NR	785, 1064	NR	32.58 (808 nm), 27.85 (1064nm)	HeLa (0~150 μg/ml, 24 h) 4T1 (0~150 μg/ml, 24 h)	76%, 82%
Dai 2021 (8)	Lip (DPQ+2DG)	Sphere	100	FI	1015	1300	0.02	26.7 (1064nm)	4T1 (0~625 μg/mL, 24 h)	75.03%
Li 2020 (9)	FS-GdNDs	NR	9.3 ± 0.5	FI	NR	NR	NR	NR	4T1 (0~5 μg/ml, NR)	85%
Wang 2019 (10)	N-B-GQDs	NR	4.7	FI	NR	1000	1.00	NR	4T1 (0~500 μg/ml, 72 h)	94%
Zheng 2021 (14)	HSC-2	Jujube	142.2	PAI/ FI	NR	957	0.41	2.01	4T1 (0~400 μg/ml, 24 h)	85%
Zheng 2020 (15)	Ag <sub>2</sub> S-GOx@BHS Nys	Sphere	91.87	FI/ PAI	NR	NR	NR	NR	4T1 (0~1000 μg/ml, 24 h)	75%
Zheng 2020 (16)	Bi <sub>2</sub> S <sub>3</sub> -Ag <sub>2</sub> S-DATS@BSA-N <sub>3</sub> Nys	Sphere	8.8 ± 1.2	FI/ PAI	900	1000	NR	NR	Hep2 (0~600 μg/ml, 12 h)	98.23%
Zhao 2020 (17)	QT-RGD	Sphere	34.7 ± 0.6	PAI	1042, 841	1068	0.12	NR	4T1 (0~20 μM, 24 h) NIH/3T3 (0~20 μM, 24 h)	>85%
Zhang 2020 (18)	TSSI NPs	Sphere	40	FI/ PAI	664	NR	NR	27.2 (785 nm), 3.1 (1064 nm)	4T1 (0~50 μg/ml, 24 h)	>96%
Zhang 2020 (19)	PSQPNs-DBCO	Sphere	35 ~ 85	FI	1064	1290	NR	NR	NR	NR
Zhang 2019 (20)	SPNs3	Sphere	43 ~ 57	PAI	899, 1000, 1300	1280	NR	2.54 (1064 nm)	4T1 (0~50 μg/ml, 48 h)	94%
Yin 2019 (21)	OSPA	Sphere	69.7 ± 2.3	PAI	1000	NR	NR	18 (980 nm)	4T1 (0~0.3 mg/ml, NR)	>90%
Yang 2020 (22)	L1057 NPs	Sphere	51	FI	470, 937	1057	1.25	NR	3T3 (0~50 μg/ml, 24 h) LO2 (0~50 μg/ml, 24 h) MEF (0~50 μg/ml, 24 h)	>85%
Xie 2021 (23)	PFG MPNs	Sphere	80	FI/ PAI	826	1063	NR	NR	B16F10 (0~1.250 mg/ml, 6 h)	>90%
Wang 2019 (24)	PEG-CSS@PB	Sphere	164	FI	NR	1525	NR	NR	HeLa (0~600 μg/ml, 24 h)	≈100%
Sun 2021 (25)	TTQ-MnCO NPs	Sphere	120	FI	NR	1115	NR	NR	MCF-7 (0~0.1 mg/ml, 24 h)	95%
Sun 2020 (26)	MNPH2	NR	NR	FI/ PAI	NR	609, 1006	0.20	NR	Hep-2 (0~800 μg/mL, NR)	≈100%
Shi 2018 (27)	Nano-PT	NR	NR	FI	790	NR	NR	130.3 (750 nm)	HCT116 (0~20 μM, NR)	96%
Li 2021 (28)	ETTC NPs	Sphere	59.3	FI	750	NR	3.00	NR	A549 (0~50 μg/mL, 24 h)	90%
Li 2019 (29)	NaLuF <sub>4</sub> NRs@PDA	Slavate	20 × 130	FI	NR	1525	1.37	5.09×10 <sup>5</sup> (M <sup>-1</sup> cm <sup>-1</sup> )	HeLa (0~1000 μg/ml, 24 h)	87%
Li 2019 (30)	PF	NR	90	FI	1026	1064	0.30	NR	4T1 (0~2.5 μg/ml, 24 h) HepG2 (0~2.5 μg/ml, 24 h)	85%, 91%
Li 2021 (31)	Pry-Ps@CP-PEG	Sphere	80	FI	900	1140	2.20	NR	4T1 (0~1 mg/m, NR)	≈90%
Li 2019 (32)	PFTDPP-SNAP NPs	NR	NR	PAI	NR	1060	1.8	NR	MCF-7 (0~1 mg/ml, NR)	>90%
Li 2021 (33)	BBTD-BET	Sphere	29 ± 3	FI/ PAI	780	1094	0.004	NR	MCF-7 (0~800 μg/ml, 24 h)	>90%
Hu 2019 (34)	PFTQ-PEG-Gd NPs	Sphere	105	FI/ PAI	NR	1056	0.38	10.36 (1064 nm)	NIH-3T3 (0~120 μg/ml, 24 h) 4T1 (0~120 μg/ml, 24 h)	88%, 91%, 90%

(Continued)

TABLE 1 Continued

Study	Names	Shape	Size (nm)	Type	A <sub>max</sub> (nm)	E <sub>max</sub> (nm)	QY (%)	ε (L/g.cm)	Cells Administration	Viability
Dai 2021 (35)	Lips (PTQ/GA/AIPH)	Sphere	85	FI/PAI	840	1300	NR	11.8	Hela (0~120 µg/ml, 24 h) MDA-MB-23 (0~50 µg/ml, NR) NIH-3T3 (0~50 µg/ml, NR)	85.64%, 90%
Chen 2021 (36)	P1 NPs	Sphere	96	FI	705	1257	0.10	NR	4T1 (0~40 µg/ml, 48 h)	92%
Jia 2021 (37)	HSC	Sphere	200	FI/PAI	NR	955	NR	NR	4T1 (0~400 µg/ml, 12 h)	90%
Qian 2021 (38)	HQS-Cy@P	Sphere	53	FI	986	1050	NR	NR	HUAEC (0~20 µg/ml, NR)	85%
Guan 2021 (39)	SPIO@NC	NR	60	FI	NR	NR	NR	3.35×10 <sup>4</sup> (M <sup>-1</sup> cm <sup>-1</sup> )	NR	NR
Xia 2020 (40)	DPP-BDT NPs	Sphere	90	FI/PAI	625	980	NR	3.05×10 <sup>4</sup> (M <sup>-1</sup> cm <sup>-1</sup> )	NIH-3T3 (0~25 µg/ml, 24 h)	80%
Xu 2020 (41)	P (DPP-BT/DOX) NPs	Sphere	100	FI/PAI	730	1076	0.42	NR	NIH3T3 (0~50 µg/ml, NR)	86%
Zhu 2020 (42)	PCTA-BMA-OXA (PBOXA)	Sphere	75.12 ± 2.19	FI	NR	1040	NR	NR	NR	NR
Yao 2020 (43)	SQ1	NR	NR	FI/PAI	940	980	1.70	26.16 (930 nm)	MDA-MB231 (0~512 µg/ml, 24 h)	80%
Wang 2019 (44)	NPs-DB	Sphere	120	FI	837, 930	1082	NR	NR	4T1 (0~1 mg/mL, 48h)	85%
Meng 2018 (45)	IR1048-MZ	NR	NR	FI/PAI	980	1046	0.60	NR	A549 (0~100 µg/ml, 24 h)	56%
Zheng 2021 (46)	Pt-Cu@PLL@HA	Areatus	56.2	PAI	NR	NR	NR	NR	4T1 (0~400 µg/ml, 24 h)	95%
Huang 2020 (47)	BDT-TTQ NPs	Sphere	100	FI	1064	1300	NR	NR	HeLa (0~0.75mg/ml, 48 h)	80%
Zhou 2020 (48)	H4-PEG-PT	NR	(180.0 ± 13) × (48 ± 15)	FI	800	1050	2.01	3.4	143B (0~32 µM, 48 h) L929 (0~32 µM, 48 h)	87%, 96%
Yang 2017 (49)	Ag <sub>2</sub> S NDs	NR	32.8	FI	NR	1060	1.32	30	4T1 (0~0.5 mM, 24 h)	~100%
Feng e 2019 (50)	IR-820	NR	NR	FI	NR	NR	2.521	NR	NR	NR
Zhao 2019 (51)	CPCC-Ag <sub>2</sub> SQDs	Sphere	3.44	FI/PAI	NR	1099	3.78	NR	Hela (0~400 g/ml, 24 h)	80%

A<sub>max</sub> (nm), maximum absorption wavelength; E<sub>max</sub> (nm), maximum emission wavelength; ε, extinction coefficient; NR, not report; QY, quantum yield.

included in this meta-analysis were able to image mice blood vessels with a diameter of about 0.4 mm (8, 17, 35, 36), while some even reached ~1.9 µm with a high-magnification imaging system (22). In addition, the blood vessels interacting with tumor tissues can be clearly observed by high-power imaging systems (29), which is of great meritorious for monitoring tumor changes during PTT. In most studies, signal intensities in tumor blocks, liver and spleen were highest at 12 h, 24 h, and 48 h (8, 9, 14–16, 18, 22, 28, 32–34, 36, 42), which then began to decline continuously. This indicates that the involved probes have higher selectivity for tumor and specific tissues. And the accumulated probe is excreted mainly through the hepatobiliary system.

## Effect of PTT guided by NIR-II imaging

The effect of periodic PTT is ultimately reflected in the actual change of tumor volume. In order to further analyze the effect of photothermal treatment, we collated the photothermal information of different PTA and the detailed changes condition of tumor *in vivo* (Table 3). Among the included studies, there were 17 items whose PTA photothermal conversion efficiency was greater than 40%, 20 items whose probe photothermal conversion efficiency was lower than 40%, and 6 items had no relevant records. PTT typically makes use of 1.0 w/cm<sup>2</sup> at 1064 nm (8, 14, 19, 20, 21, 25, 35–37, 46, 47) and 1.0 W/cm<sup>2</sup> at 808 nm (15–17, 23, 24, 26, 28, 31, 32, 34, 39, 42) NIR

TABLE 2 The characteristic profiles of probes for tumor imaging.

Study	Animal	Probe dose	PAI of tumor	FI of tumor	Ac	<i>In vitro</i> tissue signal
Zhang 2021 (7)	NR	NR	NR	NR	NR	NR
Dai 2021 (8)	NR	800µg/ml, iv.	NR	24 h, 6.7 times	0.402 mm	Liver>spleen>tumor, 48 h
Li 2020 (9)	Female BALB/c nude mice	NR	NR	12 h, NR	NR	Liver>spleen>tumor, 24 h
Wang 2019 (10)	Nude mice	1mg/ml 200µl, iv.	NR	NR	130 µm	Liver>kidney>spleen, 24 h
Zheng 2021 (14)	NR	20 mg/kg, iv.	12 h, 10 times	12 h, 8.34 times	NR	Liver>tumor>spleen, 24 h
Zheng 2020 (15)	BALB/c nude mice, 15-17 g	20 mg/kg, iv.	8 h, 7.5 times	8 h, 9.4 times	NR	Liver>tumor>spleen, 24 h
Zheng 2020 (16)	Female BALB/c nude mice, 6-8 w, 18-20 g	15 mg/kg, iv.	6 h, NR	6 h, NR	NR	Liver>tumor>spleen, 24 h
Zhao 2020 (17)	BALB/c mice	100 µM 200 µl, iv.	8 h, 13.8 times	5 h, 3.6 times	0.43 mm	Tumor>kidney>liver, 24 h
Zhang 2020 (18)	BALB/c nude mice	NR	NR	12 h NR	NR	Liver>spleen>tumor, 24 h
Zhang 2020 (19)	BALB/c mice, 6 w	2 mg/ml 100 µl, iv.	NR	NR	NR	NR
Zhang 2019 (20)	NR	1 mg/ml 100 µl, iv.	10 h, 2 times	NR	NR	NR
Yin 2019 (21)	NR	NR	6 h, 8 times	NR	NR	Liver, 24 h
Yang 2020 (22)	NR	500 µg/kg 80 µl, iv.	48 h, 4.3 times	NR	1.9 µm	Liver>tumor>spleen, 48 h
Xie 2021 (23)	C57BL/6 mice, 6-8 w, 18 ± 2 g	NR	24 h, 4.1 times	24 h, 6.7 times	NR	Liver>spleen, 36 h
Wang 2019 (24)	Female BALB/c mice	0.5 mg/ml, iv.	NR	NR	NR	NR
Sun 2021 (25)	NR	2 mg/ml 150 µl, iv.	NR	24 h, 8 times	0.35 mm	Spleen>liver>tumor, 26 h
Sun 2020 (26)	BALB/c mice, 6-8 w, 18-20 g	800 µg/ml 200 µl, iv.	8 h, 2.9 times	8 h, 2.2 times	NR	Liver>kidney>tumor, 24 h
Shi 2018 (27)	NR	NR	NR	2 h, NR	NR	NR
Li 2021 (28)	Female BALB/c mice, 5-6 w	1 mg/ml 200 µl, iv.	12 h, 6.8 times	12 h	NR	Liver>spleen>tumor, 12 h
Li 2019 (29)	NR	0.2 mg/ml 0.2 ml, iv.	NR	NR	45 µm	Liver>tumor, 60 h
Li 2019 (30)	BALB/c mice	NR	NR	12 h, NR	NR	Liver>lung>kidney, 24 h
Li 2021 (31)	NR	4 mg/ml 200 µl, iv.	NR	24 h, NR	NR	NR
Li 2019 (32)	Female BALB/c mice, 4-5 w	1 mg/ml, iv.	24 h, times	24 h, NR	NR	Liver>spleen>tumor, 24 h
Li 2021 (33)	NR	10 mg/ml 200 µl, iv.	NR	12 h, NR	0.675 mm	Liver>tumor>spleen, 24 h
Hu 2019 (34)	NR	1mg/ml 150µl, iv.	24 h, 4.5 times	24 h, NR	NR	Spleen>liver>tumor, 24 h
Dai 2021 (35)	NR	NR	24 h, 9.3 times	24 h, 4.2 times	0.42 mm	Spleen>liver>tumor, 36 h
Chen 2021 (36)	NR	2mg/ml 100ul, iv.	NR	24 h, 2.8 times	0.4 mm	Tumor>liver>spleen, 48 h
Jia 2021 (37)	Female Nude mice, 20 g	20mg/kg, iv.	NR	12 h, NR	NR	NR
Qian 2021 (38)	Female BALB/c mice, 5 w	8mg/kg 150µl, iv.	12 h	8 h, NR	0.705 mm	Liver, 8 h
Guan 2021 (39)	Female BALB/c mice, 6 w	20µg/ml 200µl, iv.	NR	24 h, NR	NR	Tumor>lung>liver, 48 h
Xia 2020 (40)	NR	2mg/ml 100µl, iv.	NR	20 h, 2.8 times	NR	NR
Xu 2020 (41)	NR	NR	20 h, 15 times	24 h, 9.4 times	NR	Liver>spleen>tumor, 72 h
Zhu 2020 (42)	Female BALB/c mice, 18-20 g	NR	24 h, 10.5 times	48 h, NR	NR	Liver>spleen>tumor, 48 h
Yao 2020 (43)	NR	5mg/kg, iv.	NR	12 h, NR	NR	NR
Wang 2019 (44)	BALB/c mice	0.25mg/ml 50µl, iv.	12 h, NR	5 d, NR	NR	Liver>kidney>spleen, 21 h
Meng 2018 (45)	Female BALB/C mice, 6-8 w, 15-20 g	40µg/ml 200µl, iv.	NR	14 h, NR	NR	Tumor>lung>liver, 14 h
Zheng 2021 (46)	Female BALB/c, 6-8 w, 17-19 g	15mg/kg, iv.	14 h, NR	24 h, 6 times	NR	NR
Huang 2020 (47)	BALB/c mice	2mg/ml 100µl, iv.	12 h, 13.4 times	12 h, 3.8 times	NR	NR
Zhou 2020 (48)	Female BALB/c nude mice, 6 w	400µg/ml 200µl, iv.	NR	12 h, NR	NR	Liver, 48h

(Continued)

TABLE 2 Continued

Study	Animal	Probe dose	PAI of tumor	FI of tumor	Ac	<i>In vitro</i> tissue signal
Yang 2017 (49)	BALB/c mice	50.0umol/kg iv.	NR	4 h, 3 times	NR	Tumor>liver>kidney, 24 h
Feng 2019 (50)	Female ICR mice, 6~7 w; Male BALB/c mice, 6~7 w	2mg/ml 100μl, iv.	24 h, 2.4 times	48 h, NR	2.496 μm	Liver>kidney, 48 h
Zhao 2019 (51)	NR	150μg/ml 100μl, iv.	NR	NR	NR	NR

Ac, the vessel width that the probe can present in the second near-infrared window; NR, not report.

light sources to irradiate the tumor site. And a few studies also choose other light sources according to the properties of PTA [e.g., 0.1 W/cm<sup>2</sup> at 980 nm (45), and 1 W/cm<sup>2</sup> at 915 nm (38)]. The PTA with excellent photothermal conversion efficiency can make the tumor heat up rapidly in a short time after feeling the NIR laser irradiation. The maximum temperature of PTA was higher than 43 °C in 31 studies, which could theoretically cause irreversible injury to tumors. Under the continuous photothermal treatment with a general period of 14 to 30 days, the tumor necrosis was gradually accompanied by a marked reduction in size.

Finally, we used the forest plot to analyze the curative effect of PTT based on the proportion of tumor cured cases to the total sample size. The total sample size of individual studies and the number of cases with different efficacy were further calculated by reviewed the included studies and the supplementary literatures. Of the 42 studies, 11 items confirmed that tumors could be completely ablated by photothermal treatment (15–18, 30, 33, 38, 48–51). And 20 items showed conspicuous reduction in tumor size but not complete elimination (8, 15, 16, 19, 20, 23, 25, 30, 32, 34–36, 38–41, 47, 48, 50, 51). Compared with the control group, tumors treated with periodic PTT could eventually be completely ablated with some degree of crusting [n=108, RR=7.01, 95%CI (3.04, 16.13), P<0.00001; Heterogeneity: Tau<sup>2</sup> = 0.00, Chi<sup>2</sup> = 1.93, df=10 (P=1.00), I<sup>2</sup> = 0%] (Figure 3A). At the same time, though most of the PTA did not completely ablate the tumor with the aid of PTT, but the tumor volume exhibited a prominent trend of reduction comparing with initial size [n=188, RR=8.49, 95%CI (4.64, 15.55), P<0.00001; Heterogeneity: Tau<sup>2</sup> = 0.00, Chi<sup>2</sup> = 1.62, df=19 (P=1.00), I<sup>2</sup> = 0%] (Figure 3B).

## Safety evaluation of PTT

Blood routine test can reflect the pathological changes of the body by observing the changes in the number and distribution of blood cells. In this study, 11 researches measured the blood routine of animals after PTT, and the main indexes were WBC, RBC, HGB, MCV, MCH and MCHC (7, 17–20, 22, 27, 28, 33, 34, 50). Unfortunately, we solely obtained detailed data from four researches for meta-analysis (7, 18, 33, 50), two of which were tumor mice (7, 18) and two were healthy mice (33, 50). Through data analysis, it was found that the blood routine

indexes except WBC were mostly within the reference range, indicating that PTT has high security for tumor treatment.

In order to analyze the particular changes of relevant indicators, we conducted a forest plot on the data of four researches. The changes of WBC [n=34, MD=-0.63, 95%CI (-1.45, 0.19), P=0.13; Heterogeneity: Chi<sup>2</sup> = 13.69, df=3 (P=0.003), I<sup>2</sup> = 78%] (Figure 4A) and MCV [n=34, MD=-0.42, 95%CI (-1.34, 0.49), P=0.36; Heterogeneity: Chi<sup>2</sup> = 15.85, df=3 (P=0.001), I<sup>2</sup> = 81%] levels in mice after periodic PTT had no effect (Figure 4B). The changes of RBC level in tumor mice showed no distinction from the control group, while reduced slightly in healthy mice [n=34, MD=-0.28, 95%CI (-0.53, -0.03), P=0.03; Heterogeneity: Chi<sup>2</sup> = 1.84, df=3 (P=0.61), I<sup>2</sup> = 0%] (Figure 4C). Although the trend of MCH level was different in tumor mice and healthy mice, the final aggregate effect showed no difference with the control group [n=34, MD=-0.21, 95%CI (-0.57, 0.14), P=0.24; Heterogeneity: Chi<sup>2</sup> = 9.71, df=3 (P=0.02), I<sup>2</sup> = 69%] (Figure 4D). MCHC levels were down regulated in both tumor and healthy mice after periodic PTT [n=34, MD=-14.99, 95%CI (-18.86, -11.12), P<0.00001; Heterogeneity: Chi<sup>2</sup> = 3.32, df=3 (P=0.34), I<sup>2</sup> = 10%] (Figure 4E).

## Quality score

The 42 studies were evaluated according to the study quality evaluation index of preclinical research, and the average score of 6.52 is shown in Table 4. The overall score of the researches ranged 3~9, among which 23 studies scored higher than 7 (8–10, 15, 16, 19, 21, 22, 24–26, 28, 29, 32–34, 38, 44–46, 48–50), and 19 studies scored between 3~6 (7, 14, 17, 18, 20, 23, 27, 30, 31, 35–37, 39–43, 47, 51). The main factors causing the subtraction of the research were lack of description of temperature, types of narcotic drugs, and randomization information.

## Discussion

According to relevant reports, cancer has long remained the leading cause of death worldwide (53), such as breast cancer (54), lung cancer (55), liver cancer (56), and colon cancer (57). Traditional clinical diagnosis and treatment measures can no longer meet the needs of precise targeted therapy and even



TABLE 3 The characteristic profiles of PTA for photothermal treatment.

Study	<i>In vitro</i> photothermal capacity	$\eta$ (%)	Administration	Conditions of PTT	$V_0$ (mm <sup>3</sup> )	Times (h)	Days (d)	$\Delta T$ (°C)	$T_{max}$ (°C)	Effect
Zhang 2021 (7)	100 µg/ml, 1064 nm, 6 min, $\Delta T=28^\circ C$	45.7	NR	NR	NR	NR	21	20.2	50.2	-
Dai 2021 (8)	NR, 1064 nm, 5 min, $\Delta T=45.4^\circ C$	40.92	800 µg/ml	1064 nm, 1.0 W/cm <sup>2</sup> , 10 min	NR	24	15	21.5	50	↑
Li 2020 (9)	5 µg/ml, 808 nm, 10 min, $\Delta T=15.8^\circ C$	43.99	3.5 mg/kg	808 nm, 0.96 W/cm <sup>2</sup> , 10 min	NR	12	16	18.1	49.1	-
Wang 2019 (10)	200 µg/ml, 808 nm, 5 min, $\Delta T=26.6^\circ C$	32.32	1 mg/mL 200 µl	808 nm, 1.5 W/cm <sup>2</sup> , 5 min	NR	NR	14	NR	NR	↓
Zheng 2021 (14)	400 µg/ml, 1064 nm, 5min, $\Delta T=34^\circ C$	41.41	20 mg/kg	1064 nm, 1.0 W/cm <sup>2</sup> 5 min	80	12	10	17.5	NR	-
Zheng 2020 (15)	NR	NR	20 mg/kg	808 nm, 1.0 W/cm <sup>2</sup> , 5 min	100	8	15	22.5	58.5	↓
Zheng 2020 (16)	600 µg/ml, 808 nm, 5 min, $\Delta T=36.9^\circ C$	31.60	15 mg/kg	808 nm, 1.0 W/cm <sup>2</sup> , 5 min	100	6	20	17.5	NR	-
Zhao 2020 (17)	NR	36.50	100 µM 200 µl	808 nm, 1.0 W/cm <sup>2</sup> , 10 min	20	4	21	21.7	NR	-
Zhang 2020 (18)	100×10 <sup>-6</sup> m, 660 nm, 5 min, $\Delta T=28^\circ C$	46	NR	660 nm, 0.3 W/cm <sup>2</sup> , 5 min	NR	12	15	17.5	54.8	-
Zhang 2020 (19)	125 µg/ml, 1064 nm, 5min, $\Delta T=50^\circ C$	33.4	2 mg/ml 100 µl	1064 nm, 1.0 W/cm <sup>2</sup> , 5 min	NR	24	15	NR	NR	↑
Zhang 2019 (20)	25 µg/ml, 1064 nm, 400 s, $\Delta T=44.5^\circ C$	60	1 mg/ml 100 µl	1064 nm, 1.0W/cm <sup>2</sup> , 5 min	NR	10	15	45	75.2	↑
Yin 2019 (21)	0.8 mg/ml, 1064 nm, 6 min, $\Delta T=59.5^\circ C$	30.53	NR	1064 nm, 1.0 W/cm <sup>2</sup> , 5 min	100	6	14	26.2	58.2	-
Yang 2020 (22)	100 µg/ml, 980 nm, 500 s, $\Delta T=27.3^\circ C$	38	500 µg/kg 80 µl	980 nm, 0.72W/cm <sup>2</sup> , 10 min	100	1	14	24	58	↓
Xie 2021 (23)	0.25 mg/ml, 808 nm, 10 min, $\Delta T=73^\circ C$	75.60	NR	808 nm, 1.0 W/cm <sup>2</sup> , 4 min	80	24	14	18.5	50	↑
Wang 2019 (24)	600 µg/ml, 808 nm, 10 min, $\Delta T=23^\circ C$	50.50	0.5 mg/ml	808 nm, 1.0 W/cm <sup>2</sup> , 10 min	90	NR	13	NR	42	↓
Sun 2021 (25)	0.10 mg/ml, 1064 nm, 5min, $\Delta T=44.8^\circ C$	44.43	2 mg/ml 150 µl	1064 nm, 1.0 W/cm <sup>2</sup> , 5 min	NR	NR	15	23.5	56	↓
Sun 2020 (26)	200 µg/ml, 808 nm, 5 min, $\Delta T=30.8^\circ C$	NR	800 µg/ml 200 µl	808 nm, 1.0 W/cm <sup>2</sup> , 5 min	100	8	16	25	59.2	-
Shi 2018 (27)	NR, 10 min, $\Delta T=32^\circ C$	27.80	NR	785 nm, 1.66 W/cm <sup>2</sup> , 5 min	NR	2	15	30.9	60.9	-
Li 2021 (28)	50 µg/ml, 808 nm, 8 min, $\Delta T=58^\circ C$	52.80	1 mg/ml 200 µl	808 nm, 1.0 W/cm <sup>2</sup> , 10 min	100	12	14	27	NR	-
Li 2019 (29)	0.2 mg/ml, 808 nm, 10 min, $\Delta T=34^\circ C$	40.18	0.2 mg/ml 0.2 ml	808 nm, 10 min	NR	NR	12	NR	NR	-
Li 2019 (30)	25 µg/ml, 808nm, 5 min, $\Delta T=29.8^\circ C$	42.30	NR	808 nm, 0.65 W/cm <sup>2</sup> , 10 min	150	1	21	20.3	51.8	-
Li 2021 (31)	1 mg/ml, 808 nm, 5 min, $\Delta T=47^\circ C$	43.70	4 mg/mL 200 µl	808 nm, 1.0 W/cm <sup>2</sup> , 5 min	80	24	15	31.5	NR	-
Li 2019 (32)	2 mg/ml, 808 nm, 10 min, $\Delta T=60^\circ C$	48	1 mg/ml	808 nm, 1.0 W/cm <sup>2</sup> , 10 min	NR	24	21	28	60	-
Li 2021 (33)	2 mg/ml, 808 nm, 5 min, $\Delta T=45.7^\circ C$	39.42	10 mg/ml 200 µl	808 nm, 0.3 W/cm <sup>2</sup> , 10 min	100	12	14	21	56	-
Hu 2019 (34)	500 µg/ml, 808 nm, 10 min, $\Delta T=41^\circ C$	26	1 mg/mL 150 µl	808 nm, 1.0 W/cm <sup>2</sup> , 10 min	80	24	16	25	58.5	↑
Dai 2021 (35)	80 µg/ml, 1064 nm, 5 min, $\Delta T=45.8^\circ C$	39.24	NR	1064 nm, 1.0 W/cm <sup>2</sup> , 10 min	NR	24	14	18	NR	↑
Chen 2021 (36)	40 µg/ml, 1064 nm, 400 s, $\Delta T=25^\circ C$	55.10	2 mg/mL 100 ul	1064 nm, 1.0 W/cm <sup>2</sup> , 5 min	100	24	15	20.7	53.2	↑

(Continued)

TABLE 3 Continued

Study	<i>In vitro</i> photothermal capacity	$\eta$ (%)	Administration	Conditions of PTT	$V_0$ (mm <sup>3</sup> )	Times (h)	Days (d)	$\Delta T$ (°C)	$T_{max}$ (°C)	Effect
Jia 2021 (37)	400 $\mu$ g/ml, 1064 nm, 5 min, $\Delta T=34^\circ\text{C}$	NR	20 mg/kg	1064 nm, 1.0 W/cm <sup>2</sup> , 5 min	100	12	10	NR	NR	-
Qian 2021 (38)	20 $\mu$ g/ml, 915 nm, 5 min, $\Delta T=24.2^\circ\text{C}$	35.50	8 mg/kg 150 $\mu$ l	915 nm, 1.0 W/cm <sup>2</sup> , 10 min	100	8	15	21.7	48	-
Guan 2021 (39)	20 $\mu$ g/ml, 808 nm, 5 min, $\Delta T=30^\circ\text{C}$	12.91	20 $\mu$ g/ml 200 $\mu$ l	808 nm, 1.0 W/cm <sup>2</sup> , 5 min	500	24	14	16.9	50.1	-
Xia 2020 (40)	100 $\mu$ g/ml, 660 nm, 10 min, $\Delta T=26^\circ\text{C}$	23	2 mg/ml 100 $\mu$ l	660 nm, 0.3 W/cm <sup>2</sup> , 10 min	100	20	14	NR	50	↑
Xu 2020 (41)	100 $\mu$ g/ml, 730 nm, 10 min, $\Delta T=45^\circ\text{C}$	50.00	NR	730 nm, 1.0 W/cm <sup>2</sup> , 10 min	NR	24	14	NR	54	↑
Zhu 2020 (42)	80 $\mu$ M, 808 nm, 10 min, $\Delta T=62^\circ\text{C}$	NR	NR	808 nm, 1.0 W/cm <sup>2</sup> , 10 min	50	24	16	18.2	53.7	↑
Yao 2020 (43)	1 mg/ml, 915 nm, 5 min, $\Delta T=41.2^\circ\text{C}$	25.60	5 mg/kg	915 nm, 0.5 W/cm <sup>2</sup> , 5 min	NR	12	14	25.9	59.1	-
Wang 2019 (44)	0.1 mg/ml, 915 nm, 6 min, $\Delta T=40^\circ\text{C}$	58.20	0.25 mg/mL 50 $\mu$ l	915 nm, 0.5 W/cm <sup>2</sup> , 10 min	120	6	15	48	68	↑
Meng 2018 (45)	100 $\mu$ g/ml, 808 nm, 5 min, $\Delta T=37^\circ\text{C}$	20.20	40 $\mu$ g/mL 200 $\mu$ l	980 nm, 0.1W/cm <sup>2</sup> , 2 min	100	14	30	30	57	-
Zheng 2021 (46)	400 $\mu$ g/ml, 1064 nm, 5 min, $\Delta T=36^\circ\text{C}$	NR	15 mg/kg	1064 nm, 1.0 W/cm <sup>2</sup> , 5 min	75	12	12	17.89	51.9	-
Huang 2020 (47)	1 mg/ml, 1064 nm, 5 min, $\Delta T=35^\circ\text{C}$	NR	2 mg/mL 100 $\mu$ l	1064 nm, 1.0 W/cm <sup>2</sup> , 5 min	100	12	15	24.5	52	↑
Zhou 2020 (48)	64 $\mu$ M, 808 nm, 12 min, $\Delta T=30.5^\circ\text{C}$	18	400 $\mu$ g/ml 200 $\mu$ l	808 nm, 1.5 W/cm <sup>2</sup> , 8 min	800	12	14	34.8	67.8	↓
Yang 2017 (49)	1.0 mM, 808 nm, 5 min, $\Delta T=35^\circ\text{C}$	35.0	50.0 $\mu$ mol/kg	785 nm, 1.5 W/cm <sup>2</sup> , 5 min	60	24	30	19.0	NR	-
Feng 2019 (50)	500 $\mu$ g/ml, 793 nm, 3 min, $\Delta T=70.5^\circ\text{C}$	32.74	2 mg/ml 100 $\mu$ l	793 nm, 2.0 W/cm <sup>2</sup> , 10 min	120	48	16	24.7	55.4	↑
Zhao 2019 (51)	600 $\mu$ g/ml, 808 nm, 6 min, $\Delta T=45^\circ\text{C}$	21	150 $\mu$ g/ml 100 $\mu$ l	808 nm, 2.5 W/cm <sup>2</sup> , 10min	100	NR	18	61.2	61.2	↑

↑, tumor volume increases; ↓, tumor reduced in size but did not disappear completely; -, complete tumor ablation;  $\eta$ , photothermal conversion efficiency;  $\Delta T$ , tumor temperature changes after laser irradiation; Days, treatment cycle; NR, not report; Times, the time at which the NIR laser irradiation began after the probe was given;  $T_{max}$ , maximum temperature of tumor after laser irradiation;  $V_0$ , the initial volume of tumor.

individualized treatment for these cancers (12). Although the commonly used measures PET, CT, MRI and US have made great achievements in tumor detection, the inevitable problems of low resolution, shallow imaging depth and certain radiation to organisms make people have to explore more excellent precise diagnosis strategies. Therefore, the optical imaging technology with high sensitivity and biological safety has been developed rapidly. Compared with visible light (400-700 nm) and NIR-I imaging, NIR-II technique with higher penetration depth and lower scattering has been generally accepted by researchers (10). It has been pronounced that the penetration depth of NIR-II imaging can reach more than 7 mm (58), contributing to identify and distinguish tiny tumors that cannot be discerned by traditional imaging strategies (59).

Conventional tumor diagnostic equipment is difficult to be integrated into the operating room and unable to provide real-time feedback of anatomical site information for aggressive surgery. Inconceivably, NIR-II guided tumor excision has

conquered this conundrum in laboratory animals because of its wide imaging field and real-time feedback of tumor sites (60–62). Stupendously, the distinctive photothermal properties of some NIR-II probes enabled to convert light energy into heat under NIR laser irradiation, thereby inducing apoptosis of tumor cells. Robust evidence has manifested that NIR-II-guided PTT has unique advantages in accurate diagnosis and non-invasive treatment of tumors in comparison with chemotherapy and surgical resection (63).

Qualified NIR probes with good biocompatibility and excellent fluorescence performance can be divided into two categories: organic materials and inorganic materials. The former includes molecule fuels, aggregation induced emission molecules and nano-polymers, while the latter comprises quantum dots, single wall nanotubes and rare earth nanoparticles (64). The luminance of the contrast agent in the NIR-II region is proportional to the product of QY and  $\epsilon$  at the excitation wavelength (22). Inorganic probes generally have high

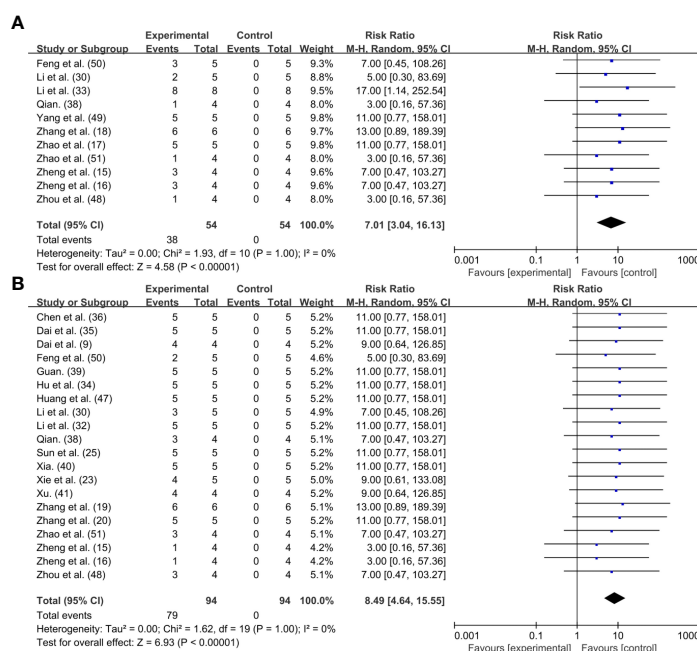


FIGURE 3

Forest plot for PTT effect: (A) Tumor disappeared completely; (B) Tumor shrank but did not completely disappear.

QY and photobleaching properties, but most of them have potential biological toxicity with the presence of toxic metal ions (65, 66). Although the biosafety of most organic fluorophores is better than that of inorganic materials, the short tumor residence time, low water solubility and QY prevent their widespread use. The lack of clinically approved NIR-II probes with high luminance and biosafety, and the inability to construct new PTA on this basis, is the main bottleneck that limit the development of PTT (67). However, the design philosophy based on structural modification and enhancement have made some progress in both safety and fluorescence properties of organic small molecules (68). A small molecule organic probe IR-820 (50) with high QY ( $\epsilon=30$  L/g-cm, QY=2.52%), reportedly showed unrivalled fluorescence brightness and could accurately image cerebral vessels at depth of 800  $\mu\text{m}$  (Figure 5A). The semiconductor polymer L1057 NPs ( $\epsilon=18$  L/g-cm, QY=1.25%) can visualize 1.9  $\mu\text{m}$  blood vessels under high power microscope (22). In addition, the probe NaLuF<sub>4</sub> NR<sub>5</sub>@PDA (29) with exceptional fluorescence emission and QY, can even illuminate the tiny blood vessels connected to the tumor with extreme clarity (Figure 5B).

The accuracy of NIR-II system in tumor diagnosis is determined by specific probes for tumor recognition. The massive accumulation of NIR-II probes at the tumor cell proclaimed intensive signal than that of surrounding tissue, which is conducive to the effective identification of tumors. Acknowledgedly, the local interactions between tumor cells

and their adjacent tissues make tumor microenvironment (TME) slight acidity and overexpression of H<sub>2</sub>O<sub>2</sub> (69). In the circumstances, Ag<sub>2</sub>S-GOx@BHS NYS, a TME specific activated probe, accumulated and ignited heterogeneous tumor (15). As a crucial organelle of ion metabolism, mitochondria are also the focus of NIR-II probe design for targeted tumor imaging. H4-PEG-PT was successfully designed to selectively capture and track mitochondria of osteosarcoma cells with a subcellular resolution of 1 nM (48). In addition, the enhanced permeability and retention effect also provides an opportunity for NIR-II probe to light the tumor through aggregated luminescence, such as PCTA-BMA-OXA (42) and SPIO@NC (39).

The selection of laser light source, the time of laser irradiation and the period of treatment are all considered as potential factors during PTT. In order to reduce the injury of laser to skin, the photothermal treatment generally chooses the laser with lower than maximum permissible exposure (33) as the irradiation light (e.g., 0.3 W/cm<sup>2</sup> at 808 nm and 1 W/cm<sup>2</sup> at 1064 nm). In the analysis of this paper, it was found that the start time of laser irradiation was generally determined by the emergence time of the maximum fluorescence or photoacoustic signal of the probe *in vivo*. The photothermal transformation of the probe could be achieved to the maximum extent when the accumulation quantity of the probe reached the utmost in the tumor tissue (Figures 5C–F). As a PTA converting light energy

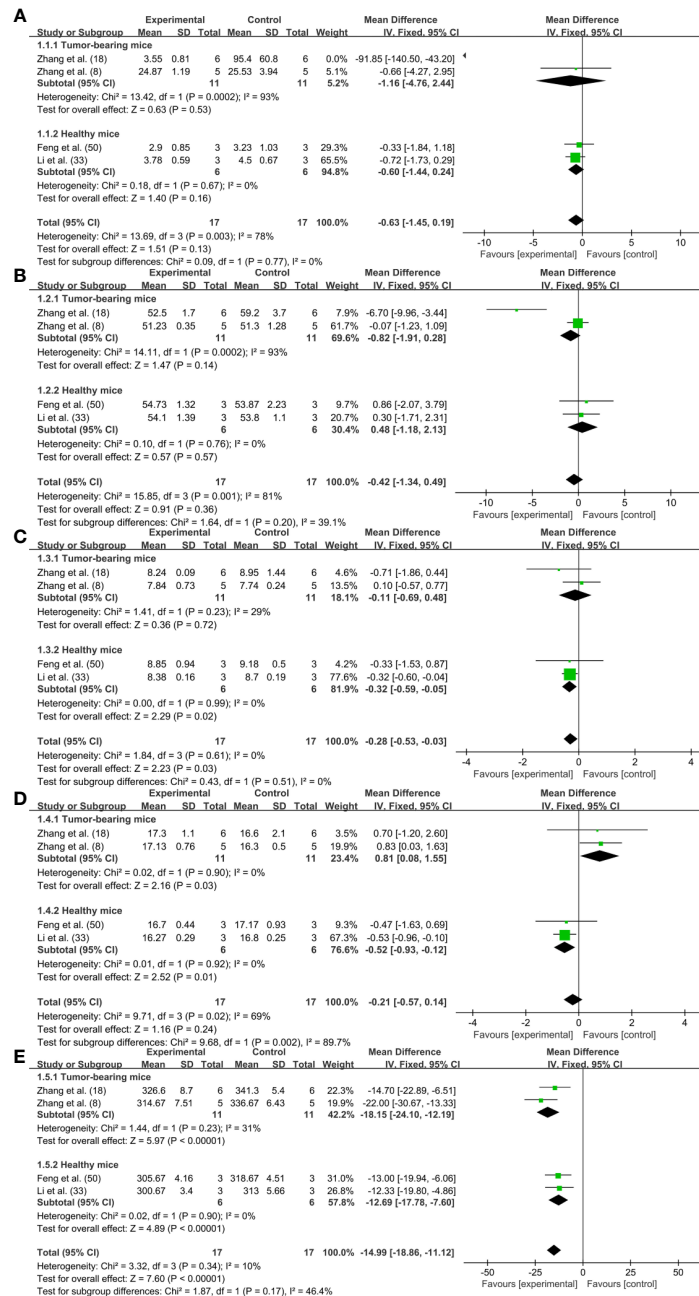


FIGURE 4  
Forrest plots for blood routine: (A) WBC; (B) RBC; (C) MCV; (D) MCH; (E) MCHC.

into heat to kill tumor cells, no applicable rules declared the period of PTT in the included studies, which should be further investigated (70). When the NIR-II probe is excited to make the local tissue temperature of tumor exceed 43°C, it will produce irreversible effect of killing tumor cells (7). At present, other than affecting mitochondrial metabolism, there is no definite conclusion on the specific mechanism of PTT.

Evidence has suggested that PTT can activate TRPV1 ion channel in tumor cells and heighten the intracellular Ca<sup>2+</sup> level, causing mitochondrial dysfunction and apoptosis (71). Thereupon, dysfunctional mitochondria can further whittle the body's resistance to thermal damage by stimulating the expression of heat shock proteins (72). Promisingly, the especially designed PTA can generally kill tumors by

TABLE 4 Quality assessment of the experiments included in the studies.

Study	1	2	3	4	5	6	7	8	9	10	Total
Zhang 2021 (7)	+	NR	NR	+	+	NR	+	+	NR	+	6
Dai 2021 (8)	+	NR	+	+	+	NR	+	+	+	+	8
Li 2020 (9)	+	NR	+	+	+	+	+	+	+	+	9
Wang 2019 (10)	+	NR	+	+	+	+	+	+	+	NR	8
Zheng 2021 (14)	+	NR	NR	+	+	NR	+	+	NR	+	6
Zheng 2020 (15)	+	NR	NR	+	+	NR	+	+	+	+	7
Zheng 2020 (16)	+	NR	NR	+	+	NR	+	+	+	+	7
Zhao 2020 (17)	+	NR	NR	+	+	NR	+	+	NR	+	6
Zhang 2020 (18)	+	NR	NR	+	+	NR	+	+	NR	+	6
Zhang 2020 (19)	+	NR	+	+	+	NR	+	+	NR	+	7
Zhang 2019 (20)	+	NR	NR	+	+	NR	+	+	NR	+	6
Yin 2019 (21)	+	NR	NR	+	+	NR	+	+	+	+	7
Yang 2020 (22)	+	NR	+	+	+	+	+	+	+	+	9
Xie 2021 (23)	+	NR	NR	+	+	NR	+	+	NR	+	4
Wang 2021 (24)	+	NR	+	+	+	-	+	+	+	+	8
Sun 2021 (25)	+	NR	+	+	+	NR	+	+	NR	+	7
Sun 2020 (26)	+	NR	+	+	+	+	+	+	+	+	9
Shi 2018 (27)	+	NR	NR	+	+	NR	+	+	NR	+	6
Li 2021 (28)	+	NR	NR	+	+	NR	+	+	+	+	7
Li 2019 (29)	+	NR	+	+	+	NR	+	NR	+	+	7
Li 2019 (30)	+	NR	+	NR	+	NR	+	+	NR	+	6
Li 2021 (31)	+	NR	NR	NR	+	NR	+	NR	NR	+	4
Li 2019 (32)	+	NR	NR	+	+	NR	+	+	+	+	7
Li 2021 (33)	+	NR	+	NR	+	+	+	+	NR	+	7
Hu 2019 (34)	+	NR	+	+	+	NR	+	NR	+	+	7
Dai 2021 (35)	+	NR	+	NR	+	NR	+	+	NR	+	6
Chen 2021 (36)	+	NR	+	NR	+	NR	+	+	NR	+	6
Jia 2021 (37)	+	NR	NR	+	+	NR	+	NR	+	NR	5
Qian 2021 (38)	+	NR	+	+	+	NR	+	+	+	NR	7
Guan 2021 (39)	+	NR	NR	NR	+	NR	+	+	NR	NR	4
Xia 2020 (40)	+	NR	+	+	+	NR	+	+	NR	NR	6
Xu 2020 (41)	+	NR	+	+	+	NR	+	NR	NR	NR	5
Zhu 2020 (42)	+	NR	+	+	+	NR	+	+	NR	NR	6
Yao 2020 (43)	+	NR	NR	NR	+	NR	+	+	NR	+	4
Wang 2019 (44)	+	NR	+	+	+	+	+	+	+	NR	8
Meng 2018 (45)	+	+	NR	+	+	+	+	+	NR	NR	7
Zheng 2021 (46)	+	NR	+	+	+	NR	+	+	+	NR	7
Huang 2020 (47)	+	NR	NR	NR	+	NR	+	+	NR	NR	3
Zhou 2020 (48)	+	NR	+	+	+	+	+	+	NR	NR	7
Yang 2017 (49)	+	NR	NR	+	+	+	+	NR	+	+	7
Feng 2019 (50)	+	+	+	+	+	NR	+	+	+	+	9
Zhao 2019 (51)	+	NR	+	NR	+	NR	+	+	NR	+	6

1, peer-reviewed publication; 2, statements describing control of temperature; 3, randomization to treatment group; 4, allocation concealment; 5 blinded assessment of outcome; 6, avoidance of anesthetics with known notable intrinsic neuroprotective properties; 7, use of animals with relevant comorbidities; 8, sample size calculation; 9, compliance with animal welfare regulations; 10, declared any potential conflict of interest +: The article confirms the indicator and gets a point. -: This article does not meet this indicator and this indicator is not scored. NR: No description of the indicator in the article.

heating up to more than 43°C in a quick time after sensing NIR laser at the tumor site (Figure 5G). Most NIR-II probes with properly photothermal properties such as TSSI NPs (18), can even achieve tumor ablation completely (Figure 5H).

It should be noticed that PTT is often distinguished from photodynamic therapy (PDT) due to the fact it does not directly depend on cellular oxygen tension. PDT principally relies on photosensitizers to generate reactive oxygen species under light

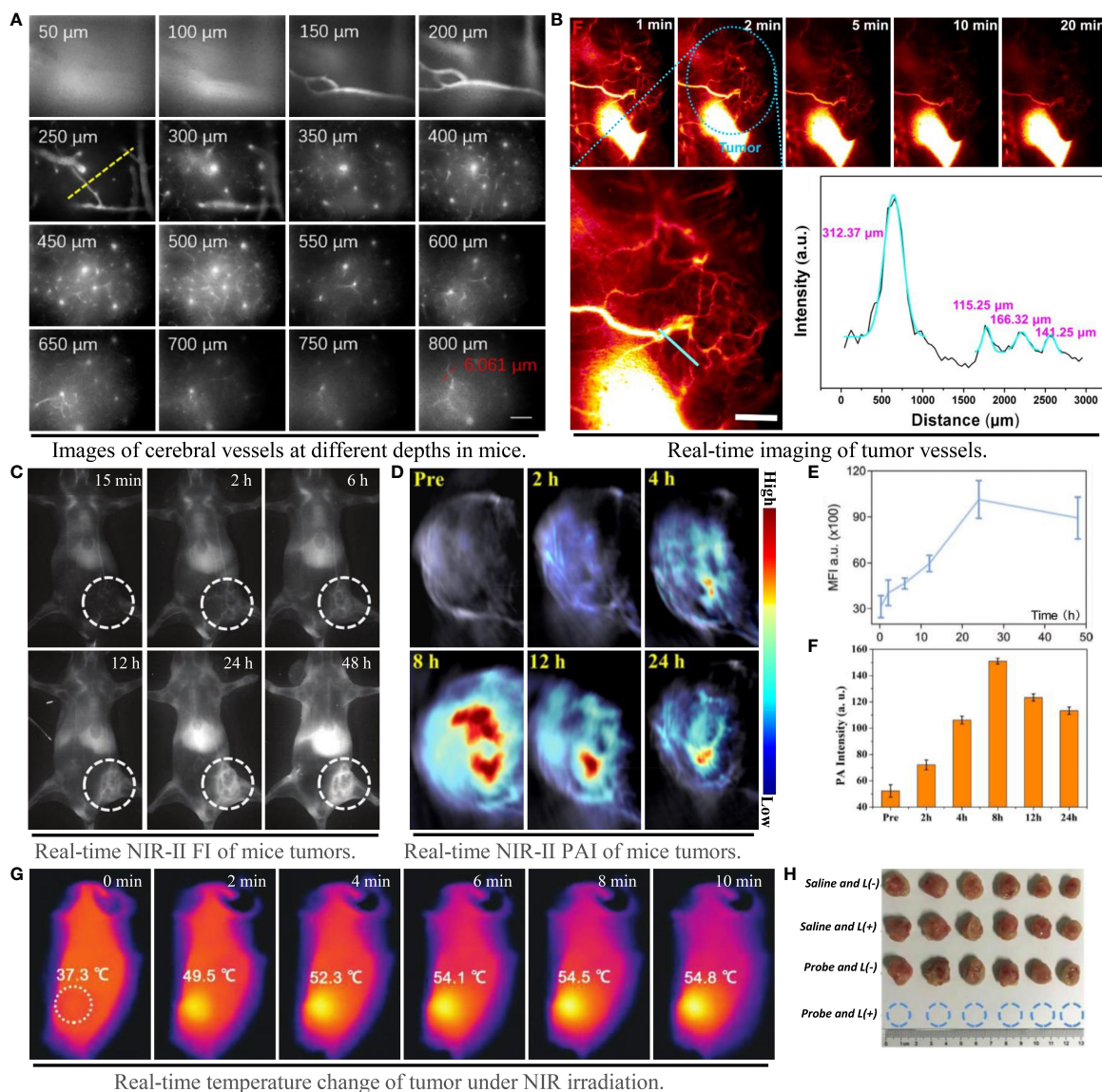


**FIGURE 5** Imaging capability of NIR-II probe on blood vessels and tumors, and effect of photothermal therapy. (A) Probe IR-820 imaging of cerebral blood vessels in mice at different tissue depths (scale bar: 100  $\mu\text{m}$ ) (50); (B) High resolution imaging of tumor vessels at magnification and gaussian fitting curve of vessel cross section (scale bar: 2 mm) (29); (C–E) NIR-II fluorescence imaging and fluorescence intensity of mouse tumors at different time points (31); (D–F) NIR-II photoacoustic imaging and photoacoustic intensity of mouse tumors at different time points (26); (G) Tumor temperature changes at different time points under NIR laser irradiation (18); (H) Tumor photos and volume changes after photothermal treatment under different conditions, from top to bottom: 1) saline; 2) saline + laser; 3) TSSI NPs; 4) TSSI NPs + laser (18).

irradiation to induce tumor cell death (73). In view of the divergent mechanisms of these two methods, PTT may be more suitable for the treatment of some hypoxic tumor, while PDT is inclined to most effective for hyperoxia tumor (74). Moreover, the intensity of the NIR laser attenuates extensively with the depth of penetration, resulting in a sudden drop in available heat energy for deep tumor mass. This limitation makes PPT more suitable for subcutaneous or other tumors closer to the body surface. In order to amplify the applicability of PTT, the combination of photothermal treatment

and PDT, immunotherapy, chemotherapy and gene therapy has been established and achieved remarkable results (75–78).

In this paper, we determined some evidence about the efficacy and safety of PTT for cancer remedy using a meta-analysis method. Whereas there are still some tricky problems need to be solved. First of all, the small sample size and some ineluctable low-quality preclinical researches have discounted the consequences of the meta-analysis to some extent. Secondly, the data available for forest plot analysis is too scarce, so we solely used the cases of

tumor complete ablation and suppression for correlation analysis. The influence of treatment conditions such as NIR laser intensity and irradiation time needs to be analyzed with more complete research data. Although NIR-II guided PTT is a promising strategy for cancer treatment, there are still many bottlenecks urgently need to be addressed before its clinical application. Sanguinely, we hold that the continuous development of NIR-II imaging technology and nanotechnology will eventually overcome the existing issues and bring more extensive application of PTT in the future.

## Conclusions

Based on a meta-analysis of preclinical studies, this paper demonstrated that PTT guided by NIR-II imaging has terrific efficacy and high safety in cancer treatment. Evidence from multiple preclinical data indicated that PTT will be a promising strategy for clinical multi-cancer therapy. Nevertheless, the development of novel NIR-II probes that are more suitable for clinical use is still the core issue of PTT therapy. Meanwhile, the potential multiorgan toxicity of probes also requires extensive preclinical and clinical evaluation.

## Author contributions

The main conception and design of this paper: FF, YaZ, XM, and XW. Data extraction and sorting: FF, YaZ, YZe, YZh and SZ.

## References

- Mun EJ, Babiker HM, Weinberg U, Kirson ED, Von Hoff DD. Tumor-treating fields: A fourth modality in cancer treatment. *Clin Cancer Res* (2018) 24:266–75. doi: 10.1158/1078-0432.ccr-17-1117
- Liu Y, Li Y, Koo S, Sun Y, Liu Y, Liu X, et al. Versatile types of Inorganic/Organic NIR-IIa/IIb fluorophores: From strategic design toward molecular imaging and theranostics. *Chem Rev* (2022) 122:209–68. doi: 10.1021/acs.chemrev.1c00553
- Zhang X, An L, Tian Q, Lin J, Yang S. Tumor microenvironment-activated NIR-II reagents for tumor imaging and therapy. *J Mater Chem B* (2020) 8:4738–47. doi: 10.1039/d0tb00030b
- Jiang Y, Li J, Zhen X, Xie C, Pu K. Dual-peak absorbing semiconducting copolymer nanoparticles for first and second near-infrared window photothermal therapy: A comparative study. *Adv Mater* (2018) 30:e1705980. doi: 10.1002/adma.201705980
- Zhang W, Cai K, Li X, Zhang J, Ma Z, Foda MF, et al. Au hollow nanorods-chimeric peptide nanocarrier for NIR-II photothermal therapy and real-time apoptosis imaging for tumor theranostics. *Theranostics* (2019) 9:4971–81. doi: 10.7150/thno.35560
- Li J, Li W, Xie L, Sang W, Wang G, Zhang Z, et al. A metal-polyphenolic nanosystem with NIR-II fluorescence-guided combined photothermal therapy and radiotherapy. *Chem Commun (Camb)* (2021) 57:11473–6. doi: 10.1039/d1cc04628d
- Zhang Y, Shen Q, Li Q, He P, Li J, Huang F, et al. Ultrathin two-dimensional plasmonic PtAg nanosheets for broadband phototheranostics in both NIR-I and NIR-II biowindows. *Adv Sci (Weinh)* (2021) 8:e2100386. doi: 10.1002/advs.202100386
- Dai Y, Sun Z, Zhao H, Qi D, Li X, Gao D, et al. NIR-II fluorescence imaging guided tumor-specific NIR-II photothermal therapy enhanced by starvation

Article drafting: FF and YH. Modification and optimization: FF and XW. All authors contributed to the article and approved the submitted version.

## Funding

This study was supported by the National Natural Science Foundation of China (82104533 and 81973569), the Science & Technology Department of Sichuan Province (2021YJ0175), and the China Postdoctoral Science Foundation (2020M683273).

## Conflict of interest

The authors declare that the research was conducted in the absence of any commercial or financial relationships that could be construed as a potential conflict of interest.

## Publisher's note

All claims expressed in this article are solely those of the authors and do not necessarily represent those of their affiliated organizations, or those of the publisher, the editors and the reviewers. Any product that may be evaluated in this article, or claim that may be made by its manufacturer, is not guaranteed or endorsed by the publisher.

mediated thermal sensitization strategy. *Biomaterials* (2021) 275:120935. doi: 10.1016/j.biomaterials.2021.120935

9. Li F, Li T, Zhi D, Xu P, Wang W, Hu Y, et al. Novel ultrasmall multifunctional nanodots for dual-modal MR/NIR-II imaging-guided photothermal therapy. *Biomaterials* (2020) 256:120219. doi: 10.1016/j.biomaterials.2020.120219

10. Wang H, Mu Q, Wang K, Revia RA, Yen C, Gu X, et al. Nitrogen and boron dual-doped graphene quantum dots for near-infrared second window imaging and photothermal therapy. *Appl Mater Today* (2019) 14:108–17. doi: 10.1016/j.apmt.2018.11.011

11. Liu H, Li C, Qian Y, Hu L, Fang J, Tong W, et al. Magnetic-induced graphene quantum dots for imaging-guided photothermal therapy in the second near-infrared window. *Biomaterials* (2020) 232:119700. doi: 10.1016/j.biomaterials.2019.119700

12. Yu H, Ji M. Recent advances of organic near-infrared II fluorophores in optical properties and imaging functions. *Mol Imaging Biol* (2021) 23:160–72. doi: 10.1007/s11307-020-01545-1

13. Vu Q, Xie K, Eckert M, Zhao W, Cramer SC. Meta-analysis of preclinical studies of mesenchymal stromal cells for ischemic stroke. *Neurology* (2014) 82:1277–86. doi: 10.1212/wnl.0000000000000278

14. Zheng Z, Jia Z, Qin Y, Dai R, Chen X, Ma Y, et al. All-in-One zeolite-Carbon-Based nanotheranostics with adjustable NIR-II window Photoacoustic/Fluorescence imaging performance for precise NIR-II photothermal-synergized catalytic antitumor therapy. *Small* (2021) 17:e2103252. doi: 10.1002/sml.202103252

15. Zheng Z, Dai R, Jia Z, Yang X, Qin Y, Rong S, et al. Biodegradable multifunctional nanotheranostic based on Ag(2)S-doped hollow BSA-SiO(2) for

- enhancing ROS-feedback synergistic antitumor therapy. *ACS Appl Mater Interf* (2020) 12:54356–66. doi: 10.1021/acsmi.0c14855
16. Zheng Z, Chen Q, Dai R, Jia Z, Yang C, Peng X, et al. A continuous stimuli-responsive system for NIR-II fluorescence/photoacoustic imaging guided photothermal/gas synergistic therapy. *Nanoscale* (2020) 12:11562–72. doi: 10.1039/d0nr02543g
  17. Zhao M, Ding J, Mao Q, Zhang Y, Gao Y, Ye S, et al. A novel  $\alpha(v)\beta(3)$  integrin-targeted NIR-II nanoprobe for multimodal imaging-guided photothermal therapy of tumors *in vivo*. *Nanoscale* (2020) 12:6953–8. doi: 10.1039/c9nr10720g
  18. Zhang Z, Xu W, Kang M, Wen H, Guo H, Zhang P, et al. An all-round athlete on the track of phototheranostics: Subtly regulating the balance between radiative and nonradiative decays for multimodal imaging-guided synergistic therapy. *Adv Mater* (2020) 32:e2003210. doi: 10.1002/adma.202003210
  19. Zhang W, Deng W, Zhang H, Sun X, Huang T, Wang W, et al. Bioorthogonal-targeted 1064 nm excitation theranostic nanoplatform for precise NIR-IIa fluorescence imaging guided efficient NIR-II photothermal therapy. *Biomaterials* (2020) 243:119934. doi: 10.1016/j.biomaterials.2020.119934
  20. Zhang W, Sun X, Huang T, Pan X, Sun P, Li J, et al. 1300 nm absorption two-acceptor semiconducting polymer nanoparticles for NIR-II photoacoustic imaging system guided NIR-II photothermal therapy. *Chem Commun (Camb)* (2019) 55:9487–90. doi: 10.1039/c9cc04196f
  21. Yin C, Li X, Wen G, Yang B, Zhang Y, Chen X, et al. Organic semiconducting polymer amphiphile for near-infrared-II light-triggered phototheranostics. *Biomaterials* (2020) 232:119684. doi: 10.1016/j.biomaterials.2019.119684
  22. Yang Y, Fan X, Li L, Yang Y, Nuernisha A, Xue D, et al. Semiconducting polymer nanoparticles as theranostic system for near-Infrared-II fluorescence imaging and photothermal therapy under safe laser fluence. *ACS Nano* (2020) 14:2509–21. doi: 10.1021/acsnano.0c00043
  23. Xie L, Li J, Wang G, Sang W, Xu M, Li W, et al. Phototheranostic metal-phenolic networks with antiexosomal PD-L1 enhanced ferroptosis for synergistic immunotherapy. *J Am Chem Soc* (2022) 144:787–97. doi: 10.1021/jacs.1c09753
  24. Wang X, Li H, Li F, Han X, Chen G. Prussian Blue-coated lanthanide-doped core/shell/shell nanocrystals for NIR-II image-guided photothermal therapy. *Nanoscale* (2019) 11:22079–88. doi: 10.1039/c9nr07973d
  25. Sun P, Jiang X, Sun B, Wang H, Li J, Fan Q, et al. Electron-acceptor density adjustments for preparation conjugated polymers with NIR-II absorption and brighter NIR-II fluorescence and 1064 nm active photothermal/gas therapy. *Biomaterials* (2022) 280:121319. doi: 10.1016/j.biomaterials.2021.121319
  26. Sun J, Cai W, Sun Y, Guo C, Zhang R. Facile synthesis of melanin-dye nanoagent for NIR-II Fluorescence/Photoacoustic imaging-guided photothermal therapy. *Int J Nanomedicine* (2020) 15:10199–213. doi: 10.2147/ijn.s284520
  27. Shi B, Yan Q, Tang J, Xin K, Zhang J, Zhu Y, et al. Hydrogen sulfide-activatable second near-infrared fluorescent nanoassemblies for targeted photothermal cancer therapy. *Nano Lett* (2018) 18:6411–6. doi: 10.1021/acsnanolett.8b02767
  28. Li X, Fang F, Sun B, Yin C, Tan J, Wan Y, et al. Near-infrared small molecule coupled with rigidity and flexibility for high-performance multimodal imaging-guided photodynamic and photothermal synergistic therapy. *Nanoscale Horiz* (2021) 6:177–85. doi: 10.1039/d0nh00672f
  29. Li X, Jiang M, Zeng S, Liu H. Polydopamine coated multifunctional lanthanide theranostic agent for vascular malformation and tumor vessel imaging beyond 1500 nm and imaging-guided photothermal therapy. *Theranostics* (2019) 9:3866–78. doi: 10.7150/thno.31864
  30. Li T, Li C, Ruan Z, Xu P, Yang X, Yuan P, et al. Polypeptide-conjugated second near-infrared organic fluorophore for image-guided photothermal therapy. *ACS Nano* (2019) 13:3691–702. doi: 10.1021/acsnano.9b00452
  31. Li J, Xie L, Li B, Yin C, Wang G, Sang W, et al. Engineering a hydrogen-Sulfide-Based nanomodulator to normalize hyperactive photothermal immunogenicity for combination cancer therapy. *Adv Mater* (2021) 33:e2008481. doi: 10.1002/adma.202008481
  32. Li J, Jiang R, Wang Q, Li X, Hu X, Yuan Y, et al. Semiconducting polymer nanotheranostics for NIR-II/Photoacoustic imaging-guided photothermal initiated nitric oxide/photothermal therapy. *Biomaterials* (2019) 217:119304. doi: 10.1016/j.biomaterials.2019.119304
  33. Li J, Wang R, Sun Y, Xiao P, Yang S, Wang X, et al. NIR-II fluorophore with dithienylethene as an electron donor for Fluorescence/Photoacoustic dual-model imaging and photothermal therapy. *ACS Appl Mater Interf* (2021) 13:54830–9. doi: 10.1021/acsmi.1c17813
  34. Hu X, Tang Y, Hu Y, Lu F, Lu X, Wang Y, et al. Gadolinium-chelated conjugated polymer-based nanotheranostics for Photoacoustic/Magnetic Resonance/NIR-II fluorescence imaging-guided cancer photothermal therapy. *Theranostics* (2019) 9:4168–81. doi: 10.7150/thno.34390
  35. Dai Y, Zhao H, He K, Du W, Kong Y, Wang Z, et al. NIR-II excitation phototheranostic nanomedicine for Fluorescence/Photoacoustic tumor imaging and targeted photothermal-photonic thermodynamic therapy. *Small* (2021) 17:e2102527. doi: 10.1002/sml.202102527
  36. Chen Y, Sun B, Jiang X, Yuan Z, Chen S, Sun P, et al. Double-acceptor conjugated polymers for NIR-II fluorescence imaging and NIR-II photothermal therapy applications. *J Mater Chem* (2021) 9:1002–8. doi: 10.1039/d0tb02499f
  37. Jia Z. *Chemical synthesis of a novel carbon-based nanomaterials and the application in tumor diagnosis and treatment*. Taiyuan University of Technology (2021). doi: 10.27352/d.cnki.gylgu.2021.001912
  38. Qian H. *Anti-aggregation cyanine dyes used in NIR-II imaging-guided photothermal therapy*. master. University of Science and Technology of China (2021). doi: 10.27517/d.cnki.gzkju.2021.001112
  39. Guan X. *Iron oxide-based nanocomposite for dual-modality ImagingGuided chemical phototherapy and anti-tumor ImmunotherapyAgainst immune cold triple-negative breast cancer*. master. Guangzhou Medical University (2021). doi: 10.27043/d.cnki.ggzyc.2021.000248
  40. Xia B. *Construction and application of a new optical nano-diagnosis and treatment system*. master. Nanjing University of Posts and Telecommunications (2020). doi: 10.27251/d.cnki.gnjdc.2020.000157
  41. Xu J. *Novel nanotheranostic system for phototherapy guided by NIR-II fluorescence imaging*. master. Nanjing University of Posts and Telecommunications (2020). doi: 10.27251/d.cnki.gnjdc.2020.001031
  42. Zhu Q. *Second near-infrared imaging-guided tumor chemotherapy-photothermotherapy combined with immune checkpoint*. master. Inner Mongolia University (2020). doi: 10.27224/d.cnki.gnmdu.2020.000955
  43. Yao D, Wang Y, Zou R, Bian K, Liu P, Shen S, et al. Molecular engineered squaraine nanoprobes for NIR-II/Photoacoustic imaging and photothermal therapy of metastatic breast cancer. *ACS Appl Mater Interf* (2020) 12:4276–84. doi: 10.1021/acsmi.9b20147
  44. Wang X. *Synthesis of conjugated polymer OpticalDiagnostic agents for tumor therapy*. master. Nanjing University of Posts and Telecommunications. (2019). doi: 10.27251/d.cnki.gnjdc.2019.000727
  45. Meng X. Multifunctional organic small molecular probe for tumor imaging and therapy. *Univ Chin Acad Sci* (2018). Available at: [https://kns.cnki.net/kcms/detail/detail.aspx?dbcode=CDFD&dbname=CDFDLAST2018&filename=1018818565.nh&uniplatform=NZKPT&v=CmRuvQVhJB02NRU6p97pEtL\\_rwDvKoE2PVvhIRF1W\\_7pHBg5x96Egp2P2Mi5ZUOE](https://kns.cnki.net/kcms/detail/detail.aspx?dbcode=CDFD&dbname=CDFDLAST2018&filename=1018818565.nh&uniplatform=NZKPT&v=CmRuvQVhJB02NRU6p97pEtL_rwDvKoE2PVvhIRF1W_7pHBg5x96Egp2P2Mi5ZUOE)
  46. Zheng Z, Qu B, Yang X, Liu L, Zhang R. Tumor-targeted pt-Cu nanoplatform for photothermal therapy guided by the second near-infrared window photoacoustic imaging. *Chin J Of Inorganic Chem* (2021) 37:1991–2001. doi: 10.11862/CJIC.2021.238
  47. Huang T, Chen Y, Sun P, Fan Q, Huang W. Conjugated-polymer nanoparticle for NIR-II fluorescence ImagingGuiding NIR-II photothermal therapy. *Acta Polymerica Sinica* (2020) 51:346–54. doi: 10.11777/j.issn1000-3304.2019.19192
  48. Zhou H, Zeng X, Li A, Zhou W, Tang L, Hu W, et al. Upconversion NIR-II fluorophores for mitochondria-targeted cancer imaging and photothermal therapy. *Nat Commun* (2020) 11:6183. doi: 10.1038/s41467-020-19945-w
  49. Yang T, Tang Y, Liu L, Lv X, Wang Q, Ke H, et al. Size-dependent Ag(2S) nanodots for second near-infrared Fluorescence/Photoacoustic imaging and simultaneous photothermal therapy. *ACS Nano* (2017) 11:1848–57. doi: 10.1021/acsnano.6b07866
  50. Feng Z, Yu X, Jiang M, Zhu L, Zhang Y, Yang W, et al. Excretable IR-820 for *in vivo* NIR-II fluorescence cerebrovascular imaging and photothermal therapy of subcutaneous tumor. *Theranostics* (2019) 9:5706–19. doi: 10.7150/thno.31332
  51. Zhao DH, Yang XQ, Hou XL, Xuan Y, Song XL, Zhao YD, et al. *In situ* aqueous synthesis of genetically engineered polypeptide-capped Ag(2S) quantum dots for second near-infrared fluorescence/photoacoustic imaging and photothermal therapy. *J Mater Chem B* (2019) 7:2484–92. doi: 10.1039/c8tb03043j
  52. Li C, Li W, Liu H, Zhang Y, Chen G, Li Z, et al. An activatable NIR-II nanoprobe for *in vivo* early real-time diagnosis of traumatic brain injury. *Angew Chem Int Ed Engl* (2020) 59:247–52. doi: 10.1002/anie.201911803
  53. Sung H, Ferlay J, Siegel RL, Laversanne M, Soerjomataram I, Jemal A, et al. Global cancer statistics 2020: GLOBOCAN estimates of incidence and mortality worldwide for 36 cancers in 185 countries. *CA Cancer J Clin* (2021) 71:209–49. doi: 10.3322/caac.21660
  54. Xu E, Hu M, Ge R, Tong D, Fan Y, Ren X, et al. LncRNA-42060 regulates tamoxifen sensitivity and tumor development via regulating the miR-204-5p/SOX4 axis in canine mammary gland tumor cells. *Front Vet Sci* (2021) 8:654694. doi: 10.3389/fvets.2021.654694
  55. Zhang Y, Holland E, Dinh A, Au D, Sun L. Bombesin-drug conjugates in targeted therapy for small cell lung cancer. *Am J Cancer Res* (2022) 3:927–37.



56. Sas Z, Cendrowicz E, Weinhäuser I, Rygiel TP. Tumor microenvironment of hepatocellular carcinoma: Challenges and opportunities for new treatment options. *Int J Mol Sci* (2022) 23:3778. doi: 10.3390/ijms23073778
57. Wu H, Du J, Li C, Li H, Guo H, Li Z. Kaempferol can reverse the 5-fluorouracil resistance of colorectal cancer cells by inhibiting PKM2-mediated glycolysis. *Int J Mol Sci* (2022) 23:3544. doi: 10.3390/ijms23073544
58. Liu H, Wang X, Huang Y, Li H, Peng C, Yang H, et al. Biocompatible croconaine aggregates with strong 1.2–1.3  $\mu\text{m}$  absorption for NIR-IIa photoacoustic imaging *in vivo*. *ACS Appl Mater Interf* (2019) 11:30511–7. doi: 10.1021/acsami.9b06824
59. Hu Z, Fang C, Li B, Zhang Z, Cao C, Cai M, et al. First-in-human liver-tumour surgery guided by multispectral fluorescence imaging in the visible and near-infrared-I/II windows. *Nat BioMed Eng* (2020) 4:259–71. doi: 10.1038/s41551-019-0494-0
60. Yang RQ, Lou KL, Wang PY, Gao YY, Zhang YQ, Chen M, et al. Surgical navigation for malignancies guided by near-infrared-II fluorescence imaging. *Small Methods* (2021) 5:e2001066. doi: 10.1002/smt.202001066
61. Yamada Y, Ohno M, Fujino A, Kanamori Y, Irie R, Yoshioka T, et al. Fluorescence-guided surgery for hepatoblastoma with indocyanine green. *Cancers (Basel)* (2019) 11:1215. doi: 10.3390/cancers11081215
62. Yang RQ, Wang PY, Lou KL, Dang YY, Tian HN, Li Y, et al. Biodegradable nanoprobe for NIR-II fluorescence image-guided surgery and enhanced breast cancer radiotherapy efficacy. *Adv Sci (Weinh)* (2022) 9:e2104728. doi: 10.1002/advs.202104728
63. Li S, Zhang Y, Liu X, Tian Y, Cheng Y, Tang L, et al. Smart NIR-II croconaine dye-peptide for enhanced photo-sonotheranostics of hepatocellular carcinoma. *Theranostics* (2022) 12:76–86. doi: 10.7150/thno.64759
64. Xie N, Hou Y, Wang S, Ai X, Bai J, Lai X, et al. Second near-infrared (NIR-II) imaging: a novel diagnostic technique for brain diseases. *Rev Neurosci* (2022) 33:467–90. doi: 10.1515/revneuro-2021-0088
65. Li Y, Zeng S, Hao J. Non-invasive optical guided tumor Metastasis/Vessel imaging by using lanthanide nanoprobe with enhanced down-shifting emission beyond 1500 nm. *ACS Nano* (2019) 13:248–59. doi: 10.1021/acsnano.8b05431
66. Li B, Lu L, Zhao M, Lei Z, Zhang F. An efficient 1064 nm NIR-II excitation fluorescent molecular dye for deep-tissue high-resolution dynamic bioimaging. *Angew Chem Int Ed Engl* (2018) 57:7483–7. doi: 10.1002/anie.201801226
67. Zhu S, Hu Z, Tian R, Yung BC, Yang Q, Zhao S, et al. Repurposing cyanine NIR-I dyes accelerates clinical translation of near-infrared-II (NIR-II) bioimaging. *Adv Mater* (2018) 30:1802546. doi: 10.1002/adma.201802546
68. He S, Song J, Qu J, Cheng Z. Crucial breakthrough of second near-infrared biological window fluorophores: design and synthesis toward multimodal imaging and theranostics. *Chem Soc Rev* (2018) 47:4258–78. doi: 10.1039/c8cs00234g
69. Xu Z, Qian J, Meng C, Liu Y, Ding Q, Wu H, et al. TME-targeting theranostic agent uses NIR tracking for tumor diagnosis and surgical resection and acts as chemotherapeutic showing enhanced efficiency and minimal toxicity. *Theranostics* (2022) 12:2535–48. doi: 10.7150/thno.68074
70. Li X, Lovell JF, Yoon J, Chen X. Clinical development and potential of photothermal and photodynamic therapies for cancer. *Nat Rev Clin Oncol* (2020) 17:657–74. doi: 10.1038/s41571-020-0410-2
71. Ma Z, Zhang J, Zhang W, Foda MF, Zhang Y, Ge L, et al. Intracellular Ca(2+) cascade guided by NIR-II photothermal switch for specific tumor therapy. *iScience* (2020) 23:101049. doi: 10.1016/j.isci.2020.101049
72. Richter K, Haslbeck M, Buchner J. The heat shock response: life on the verge of death. *Mol Cell* (2010) 40:253–66. doi: 10.1016/j.molcel.2010.10.006
73. Ming L, Cheng K, Chen Y, Yang R, Chen D. Enhancement of tumor lethality of ROS in photodynamic therapy. *Cancer Med* (2021) 10:257–68. doi: 10.1002/cam4.3592
74. Jung HS, Verwilt P, Sharma A, Shin J, Sessler JL, Kim JS. Organic molecule-based photothermal agents: an expanding photothermal therapy universe. *Chem Soc Rev* (2018) 47:2280–97. doi: 10.1039/c7cs00522a
75. Wang Y, Luo S, Wu Y, Tang P, Liu J, Liu Z, et al. Highly penetrable and on-demand oxygen release with tumor activity composite nanosystem for Photothermal/Photodynamic synergetic therapy. *ACS Nano* (2020) 8:17046–62. doi: 10.1021/acsnano.0c06415
76. Chen Q, Xu L, Liang C, Wang C, Peng R, Liu Z. Photothermal therapy with immune-adjuvant nanoparticles together with checkpoint blockade for effective cancer immunotherapy. *Nat Commun* (2016) 7:13193. doi: 10.1038/ncomms13193
77. Ma N, Zhang M, Wang X, Zhang L, Feng J, Zhang X. NIR light-triggered degradable MoTe2 nanosheets for combined photothermal and chemotherapy of cancer. *Adv Funct Mater* (2018) 28:1801139. doi: 10.1002/adfm.201801139
78. Tao W, Cheng X, Sun D, Guo Y, Wang N, Ruan J, et al. Synthesis of multi-branched Au nanocomposites with distinct plasmon resonance in NIR-II window and controlled CRISPR-Cas9 delivery for synergistic gene-photothermal therapy. *Biomaterials* (2022) 287:121621. doi: 10.1016/j.biomaterials.2022.121621